Biochemical and Biophysical Research Communications 445 (2014) 78–83

Contents lists available at ScienceDirect

Biochemical and Biophysical Research Communications

journal homepage: www.elsevier.com/locate/ybbrc

Crystal structure of cbbF from *Zymomonas mobilis* and its functional implication

Hyo-Jeong Hwang, Suk-Youl Park, Jeong-Sun Kim *

Department of Chemistry, Chonnam National University, Gwangju 500-757, Republic of Korea

ARTICLE INFO

Article history:
Received 17 January 2014
Available online 31 January 2014

Keywords:
Crystal structure
IMPase
FBPase
cbbF
Zymomonas mobilis

ABSTRACT

A phosphate group at the C1-atom of inositol-monophosphate (IMP) and fructose-1,6-bisphosphate (FBP) is hydrolyzed by a phosphatase IMPase and FBPase in a metal-dependent way, respectively. The two enzymes are almost indiscernible from each other because of their highly similar sequences and structures. Metal ions are bound to residues on the β1- and β2-strands and one mobile loop. However, FBP has another phosphate and FBPases exist as a higher oligomeric state, which may discriminate FBPases from IMPases. There are three genes annotated as FBPases in *Zymomonas mobilis*, termed also cbbF (*Zm*cbbF). The revealed crystal structure of one *Zm*cbbF shows a globular structure formed by five stacked layers. Twenty-five residues in the middle of the sequence form an α-helix and a β-strand, which occupy one side of the catalytic site. A non-polar Leu residue among them is protruded to the active site, pointing out unfavorable access of a bulky charged group to this side. *In vitro* assays have shown its dimeric form in solution. Interestingly, two β-strands of β1 and β2 are disordered in the *Zm*cbbF structure. These data indicate that *Zm*cbbF might structurally belong to IMPase, and imply that its active site would be reorganized in a yet unreported way.

1. Introduction

Myo-inositol is a precursor for a lipid membrane component phosphatidylinositol that is especially abundant in brain tissue [1], and a hydrolyzed product of inositol-1-monophosphate (IMP) that is catalyzed by IMP phosphatases (IMPases) [2]. In bipolar disorder sufferers, the phosphatidylinositol signaling pathway is hyperactive when IMPase is inhibited, resulting in the symptomatic relief of the disorder [3].

IMPase has been proposed to show an unusual mechanism for the dephosphorylation of IMP, because, unlike most phosphatases, it does not proceed by a phospho-enzyme intermediate [4]. Instead, its catalysis may occur by assistance of two or three metal ions, where two magnesium ions may stabilize negative charges on a nucleophilic water and the leaving phosphate group [5–12].

In addition to the specificity for IMP, archaeal IMPases have also mediated the cleavage reaction of the phosphoester-bond at the C1-atom of the fructose ring of FBP in the presence of Mg^{2+} or Ca^{2+} ions. Therefore, IMPase and FBPase were suggested to evolve from the same gene product [7–8]. Accordingly, minute active site environments of IMPases and FBPases, as well as their overall structures, are very similar. A Lys residue on the mobile loop (ML) of IMPases and FBPases coordinates the Li ion, together with three acidic residues from the globular domain, which includes a Glu residue on the loop between the β1- and β2-strands (β1-β2 loop). The ML has also been suggested to take part in the product release [7,12].

However, FBP has another phosphate group attached to the C6-atom of the fructose ring, in addition to the phosphate at the C1-atom. Therefore, there would be an extra space in FBPases, compared to IMPases, to accommodate this bulky negatively-charged phosphate group. Their oligomeric states are also different: most FBPases form a higher oligomeric structure, for example, tetrameric state, whereas many eukaryotic IMPases function as a dimeric protein. In contrast, archaeal bifunctional FBPases/IMPases form a tetrameric structure [10].

Three putative FBPase genes, also named as cbbFs, are present in *Zymomonas mobilis* ZM4 [13]. In this study, we elucidated the crystal structure of one cbbF (ZMO1518) from *Z. mobilis* (*Zm*cbbF),

Abbreviations: DLS, dynamic light scattering; FBP, fructose-1,6-bisphosphate; FBPase, FBP phosphatase; IMP, inositol-monophosphate; IMPase, IMP phosphatase; ML, mobile loop; rmsd, root-mean-square-deviation; SEC, size-exclusion chromatography.

* Corresponding author. Address: Department of Chemistry, Chonnam National University, 300 Yongbong-dong, Buk-gu, Gwangju 500-757, Republic of Korea. Fax: +82 62 530 3389.

E-mail address: jsunkim@chonnam.ac.kr (J.-S. Kim).

http://dx.doi.org/10.1016/j.bbrc.2014.01.152
0006-291X/

which provides a structural clue for its catalytic specificity against IMP, rather than FBP, and suggests interesting features to implicate the enzymatic mechanism in this protein family.

2. Materials and methods

2.1. Cloning, expression, and purification of ZmcbbF

The *Z. mobilis* ZM4 gene coding for *Zm*cbbF (ZMO1518, Met1-Leu260), out of three annotated cbbFs of ZMO0329, ZMO1409, and ZMO1518 [13], was amplified using polymerase chain reaction (PCR) from the chromosomal DNA of *Z. mobilis* ZM4 with two primers designed for ligation-independent cloning [14]: 5′-ggc ggt ggt ggc ggc atg tcc cga agc gct tat gaa gat ga-3′ and 5′-gtt ctt ctc ctt tgc gcc ctt ata att cca tgg cag aca atg ctg gtt c-3′. The PCR product was treated with T4 DNA polymerase (New England Biolabs) and inserted into a vector derived from the pET21a plasmid (Novagen). This vector was designed to express the cloned gene fused to the $(His)_6$ tag and the Tobacco etch virus (TEV) cleavage sequence at the N-terminus. The *Escherichia coli* BL21(DE3)star strain transformed with the expression construct was grown in Luria Bertani medium. After induction by adding 0.5 mM Isopropyl β-D-1-thio-galactopyranoside, the culture media was maintained for 8 h at 310 K. The culture was harvested by centrifugation at 5000*g* and 277 K. The harvested cells were re-suspended and disrupted by ultra-sonication in buffer A (20 mM Tris–HCl at pH 7.5 and 500 mM NaCl). The supernatant was loaded onto a 5 ml HisTrap chelating column (GE healthcare). The column was extensively washed with buffer A and the bound proteins were eluted with a linear gradient from 0–500 mM Imidazole in buffer A. The eluted sample was dialyzed against buffer B (20 mM Tris–HCl at pH 7.5 and 300 mM NaCl) and the $(His)_6$ tag was cleaved with TEV. The protein was further purified by size-exclusion chromatography using a Superose 12 size-exclusion column (10 × 300 mm; GE healthcare, Uppsala, Sweden).

2.2. Crystallization, data collection, and structure determination

The purified protein was concentrated to 15 mg ml^{-1} in buffer B, whose concentration was determined using an extinction coefficient at 280 nm of 0.981 mg ml^{-1} cm^{-1} calculated from its amino-acid sequence. The initial crystallizing condition was obtained from Sparse Matrix Screening [15]. Suitable crystals for diffraction experiments were obtained using the hanging-drop vapor-diffusion method at 295 K within 3 d from the precipitant containing 9–11% (w/v) polyethylene glycol 4000, 0.2 M Lithium sulfate, and 0.1 M Tris–HCl at pH 8.5. For data collection, crystals were briefly immersed into a precipitant solution containing 10% (v/v) glycerol and immediately placed in a 100 K nitrogen-gas stream. One X-ray diffraction data set was collected at the 6C1 beamline of the Pohang Accelerator Laboratory (PAL) at a wavelength of 1.20 Å. The data were indexed, integrated, and scaled with HKL-2000 suite [16]. The electron density was calculated from the molecular replacement using the program PHENIX [17]. Further model building was performed manually using the program WinCoot [18] and subsequent refinement was performed with PHENIX [17]. The diffraction data and structure refinement statistics are summarized in Table 1. The quality of the model was analyzed with WinCoot and MolProbity [18,19]. Figures for the ribbon diagram and stick model were prepared using the PyMol Molecular graphics program (Delano Scientific).

2.3. Dynamic light scattering (DLS) analysis

The DLS experiments were performed at 293 K with a Microtrac's DLS model Nanotrac ULTRA (Advanced Research Tool Corp., Chicago, USA). Baseline measurement using buffer C (20 mM Tris–HCl at pH 7.5 and 100 mM NaCl) was carried out prior to the measurement of the samples. The protein concentration used was 20 μM in buffer C in a volume of 200 μl. The DLS was measured for 1 min and corrections for the buffer viscosity and protein refractive index were made using Microtrac FLEX application software.

Table 1
Data collection and structure refinement statistics.

Data collection	*Zm*cbbf
Synchrotron	5C MXII, PAL
Wavelength (Å)	1.20
Space group	$P3_221$
Cell parameters (Å, °)	$a = b = 90.75$, $c = 75.27$, $\alpha = \beta = 90$, $\gamma = 120$
Resolution (Å)	50.0 − 1.90 (1.97 − 1.90)
Completeness (%)	100.0 (100.0)
R^a_{sym} (%)	5.1 (40.1)
Reflections, observed/unique	289,055/28,603
I/Sigma (I)	11.4 (4.8)
Sigma cutoff	0
Refinement	
R^b_{factor} (%)	14.7 (16.5)
R^c_{free} (%)	17.7 (22.5)
No. of protein molecules	1
No. of atoms, protein/water	1929/294
RMSD, bonds (Å)/angles (°)	0.019/1.70
B-factors (Å^2), protein/water	21.7/34.5
Geometry (%)	
Most favored	99.2
Additionally allowed	0.8
Outliers	0
PDB ID	4n81

Values in parentheses are for the highest-resolution shell.
RMSD: root-mean-square-deviation from ideal values [18].
[a] $R_{sym} = \sum_{hkl}\sum_j|I_j - < I >|/\sum_{hkl}\sum_j I_j$, where <*I*> is the mean intensity of reflection hkl.
[b] $R_{factor} = \sum_{hkl}||Fobs| - |Fcalc||/\sum_{hkl}|Fobs|$; where *F*obs and *F*calc are, respectively, the observed and calculated structure factor amplitudes for the reflections hkl included in the refinement.
[c] R_{free} is the same as R_{factor} but calculated over a randomly selected fraction (10%) of the reflection data not included in the refinement.

2.4. Size-exclusion chromatography (SEC) analysis

The SEC analyses for the purified *Zm*cbbF were performed on an AKTA Explorer chromatography system using a Superose 12 size-exclusion column (10 × 300 mm; GE Healthcare, Sweden) with buffer C at a flow rate of 0.5 ml/min. The chromatograms were obtained by monitoring the absorbance at 280 nm. The injection amount was 40 μM *Zm*cbbF in a volume of 100 μl. A set of molecular mass standard markers (Sigma) ranging from 29 to 150 kDa was used.

3. Results and discussion

3.1. Overall features of ZmcbbF

The crystal structure of *Zm*cbbF was determined by molecular replacement using the monomeric IMPase SuhB (PDB ID 2QFL) as a search model. This SuhB has approximately 25% sequence identity to *Zm*cbbF. The refined *Zm*cbbF at a resolution of 1.9 Å shows a single globular structure that is formed with five stacked layers of α-helical bundle and β-sheet (Fig. 1). The first two amino acids at the N-terminus and residues of Gly69-Asp78 are not traced (red-dotted line in Fig. 1). A sulfate ion is found, which was probably taken from the precipitant solution during the crystallization step. Analysis of the modeled residues by MolProbity [19] showed that all residues were found in the valid regions of the Ramachandran plot (Table 1).

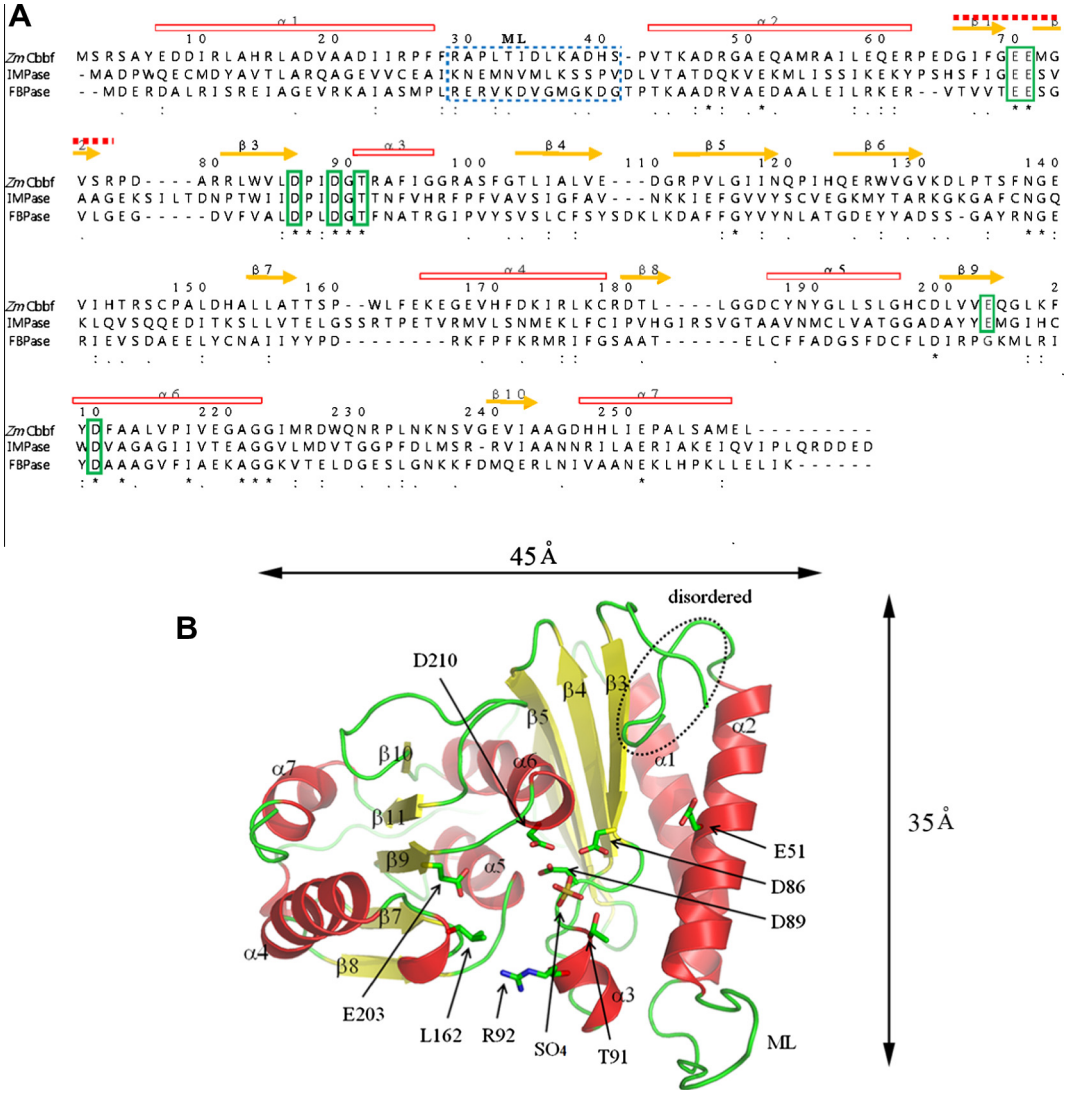

Fig. 1. Structural features of *Zm*cbbF. (A) Structure-based sequence alignment. The rectangles (α) and the arrows (β) above the aligned sequences represent the helix and the strand observed in *Zm*cbbF, respectively. The numbering scheme used follows the amino acid sequence of *Zm*cbbF. The identical residues are marked by "∗" and conserved residues by ":" and by ".". The disordered β1 and β2 region in the *Zm*cbbF structure was indicated by a continuous red-dotted line. The catalytic residues for substrate hydrolysis and metal coordination were enclosed by green boxes, while the mobile loop (ML) is by the blue-dotted box. The abbreviations used in this figure are *Zm*cbbF for cbbF from *Z. mobilis* ZM4 (PDB ID 4n81), IMPase for IMPase from human Inositol Monophosphatase (PDB ID 1IMA), and FBPase for FBPase from *A. fulgidus* (PDB ID 1LBY). The sequence alignment was prepared with ClustalW2 software from the European Bioinformatics Institute based on amino acid sequences. The figures, except for Fig. 1(A), were prepared by the PyMol Molecular graphics program of Delano Scientifics. (B) Monomeric structure. The monomeric structure of *Zm*cbbF was displayed as a ribbon diagram and the catalytic residues were by stick models. The mobile loop (ML) was marked, while the disordered β1 and β2 region in the structure was indicated by a black-dotted circle (disordered). The bound sulfate ion was displayed by stick models. The measured molecular size of the monomeric *Zm*cbbf along the longest and the shortest axes was indicated. (For interpretation of the references to color in this figure legend, the reader is referred to the web version of this article.)

A similarity search using the DALI server (http://www.ebi.ac.uk/dali) showed that *Zm*cbbF has a close structural relationship with more than 200 phosphatases, most of which belong to an IMPase and/or an FBPase superfamily. Even though the sequence identity of *Zm*cbbF to other proteins is relatively low (less than 25%), *Zm*cbbF structure is well superposed on IMPases and FBPases with root-mean-square-deviation values of less than 2 Å and 2.5 Å for the compared 230 and 210 Cα positions, respectively. Several residues responsible for catalysis in IMPases and FBPases are spatially conserved in the *Zm*cbbF structure (Fig. 2).

3.2. The active site of ZmcbbF

Due to structural similarity and sequentially- and structurally-conserved catalytic residues (Figs. 1 and 2), the putative catalytic site of *Zm*cbbF can be easily deduced. Within this site, the observed sulfate ion interacts with conserved residues of Asp86, Asp89, Thr191, and Asp210 of *Zm*cbbF (Fig. 2C). Further, its spatial position coincides with that of the phosphate group attached at the C1 atom of FBP in FBPase (Fig. 2). These structural features strongly imply that the sulfate ion-binding region might be the active site of *Zm*cbbF. Notably, the four aforementioned residues were also involved in the interactions with the phosphate group of FBP in FBPase (Fig. 2B), and the sulfate ion was also observed in the active site of the Staphylococcal dual specific IMPase/NADP(H) phosphatase [20]. Because a sulfate ion has the same number of atoms as, and a similar molecular volume to, that of the phosphate ion, the observed interaction between the protein and the sulfate ion may further represent the phosphate-binding geometry in *Zm*cbbF.

3.3. Oligomeric state of ZmcbbF

To characterize the oligomeric state of *Zm*cbbF, we performed dynamic light scattering (DLS) analysis. It showed only one major

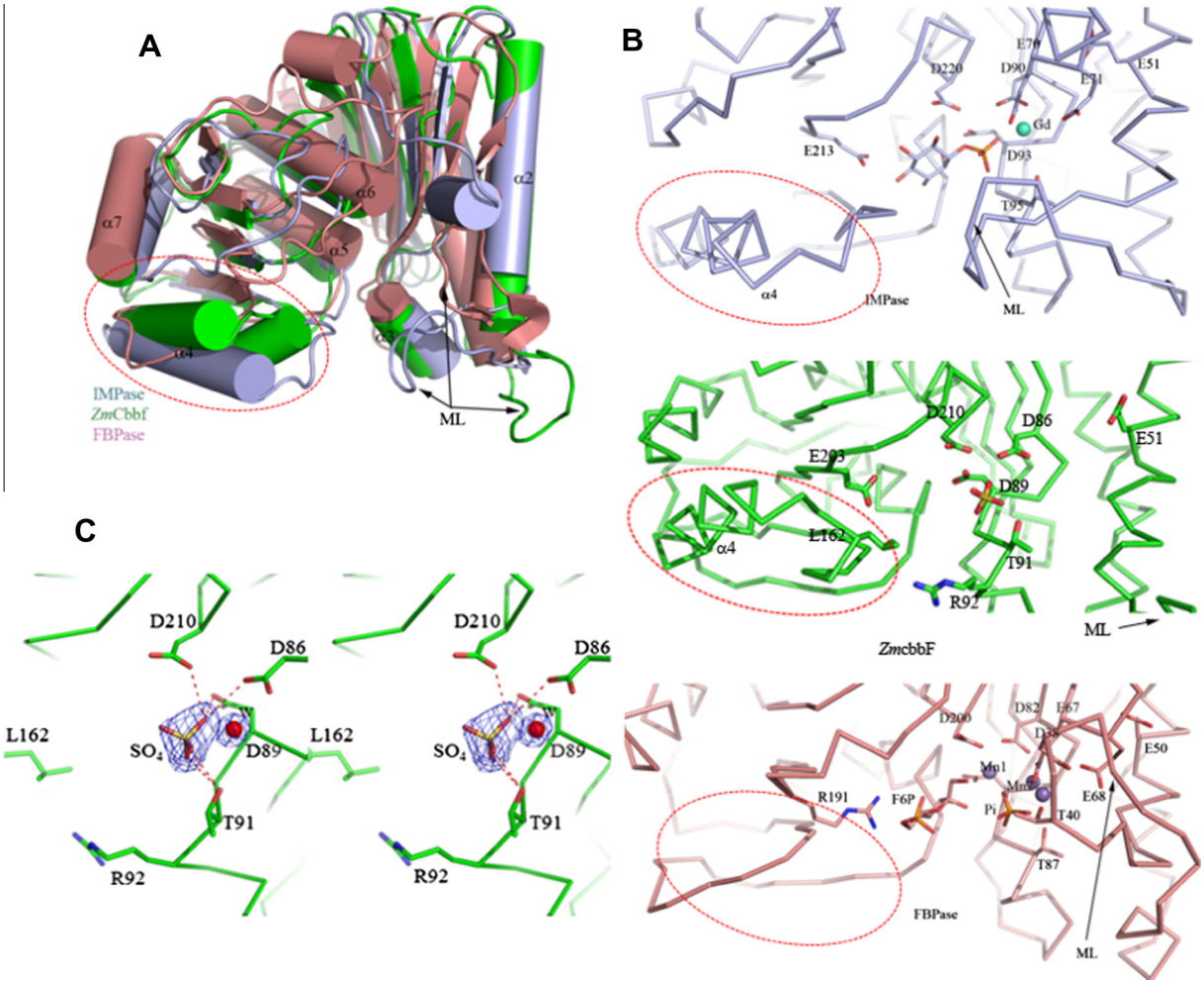

Fig. 2. Comparison with other related structures. The red-dotted circles indicate the region of the 160–190th residues. The bound metal ions were displayed as spheres and key residues and substrate/product analogs as stick models. (A) Superposition of three structurally related proteins. The α-helices and the β-strands were represented by cylinders and arrows, respectively, and three superposed molecules of *Zm*cbbF (green), IMPase from human (forest), and FBPase from *A. fulgidus* (orange) were discerned by colors. (B) Close-up view of the active site. (top) The bound Gd^{3+} ion (Gd) in IMPase was indicated. (middle) The bound sulfate ion in *Zm*cbbF was displayed with stick models. (bottom) The bound metal ions (Mn1, Mn2, and Mn3) in FBPase were displayed as spheres with fructose-6-phosphate (F6P) and orthophosphate (Pi) as stick models. (C) Stereo-presentation of the *Zm*cbbF active site. The sulfate ion (SO_4) and a water molecule (w) were displayed by stick models and a sphere, respectively, with its $2Fo - Fc$ density (blue) contoured at 1.0 σ. The hydrophilic interactions between the side chain atoms and the sulfate ion were displayed with red-dotted lines. (For interpretation of the references to color in this figure legend, the reader is referred to the web version of this article.)

peak for particles with a mean hydrodynamic radius of 59.4 ± 7.8 Å (Fig. 3A) and a suggested molecular mass of approximately 65 kDa. The estimated diameter is much larger than 45 Å along the longest axis of the monomeric *Zm*cbbF that has a theoretical molecular weight of 29 KDa (Fig. 1B). Simultaneously, data from size-exclusion chromatography showed that it was eluted just after the human serum albumin of 66 kDa and far before the carbonic anhydrase of 29 kDa (Fig. 3B), strongly indicating that size distribution in solution is close to its dimeric state.

Even though the present *Zm*cbbF structure shows a monomeric protein in the asymmetric unit (Fig. 1B), examination of symmetry-related molecules suggests a possible dimeric structure (Fig. 4, Left). The longest axis of this modeled dimeric *Zm*cbbF is approximately 60 Å, which is consistent with the diameter of 59.4 Å that was obtained from the DLS measurement (Fig. 3A). Five secondary elements (ML, the α3-β4 loop, the β5-β6 loop, the α5-helix, and the β8-α5 loop from both protomers) form a dimeric interface. Besides hydrophobic interaction, hydrophilic interactions are observed here (Fig. 4, right). Two amide-nitrogen atoms of a side chain of Arg29 on the ML in one protomer form a hydrophilic interaction with the Glu125 side chain atoms on the β5-β6 loop and the hydroxyl group of Tyr188 on the β8-α5 loop of the other protomer. The amide-atoms of the side chain of Arg98 on the α3-β4 loop of one protomer hydrophilically interact with the carbonyl oxygens of the main-chain atom of Leu183 and Gly184 on the β8-α5 loop and the carbonyl oxygen of Asn189 on the α5-helix of the other protomer.

FBPases and dual IMPase/FBPases commonly form tetrameric structures, while eukaryotic IMPases do homodimers [10]. Even the *Mycobacterium tuberculosis* IMPase that is present as a monomer forms a dimeric structure when Mg^{2+} ions are added [21]. On this regard, the observed *in vitro* dimeric state strongly indicates that *Zm*cbbF is more related to IMPases, rather than FBPases.

3.4. Comparison to other FBPases and IMPases

As mentioned above, overall structural features reported in IMPases and FBPases, including catalytic residues, are well conserved in the revealed *Zm*cbbF structure. Nonetheless, there are some intriguing sequential and structural features in *Zm*cbbF. First, approximately 25 residues between the 160th and 185th amino

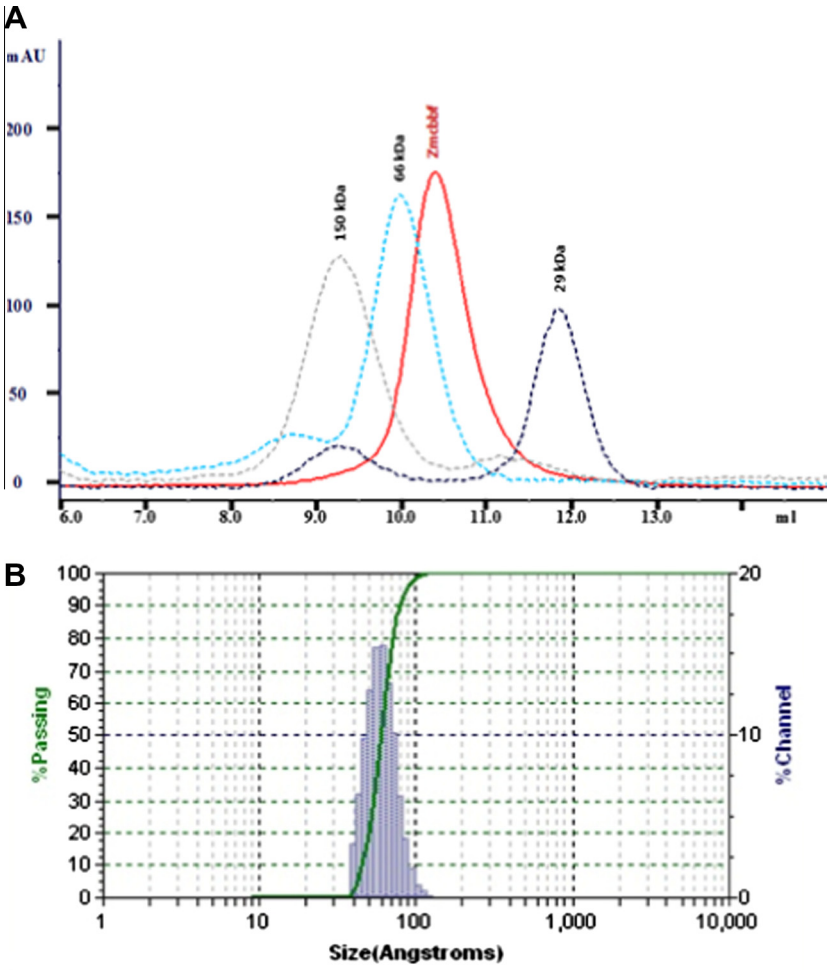

Fig. 3. Analysis of the oligomeric state. (A) DLS analysis. The calculated mean diameter of hydrodynamic and its distribution are 59.4 ± 7.8 Å (σ = 13.1%), suggesting the estimated molecular mass of approximately 65 kDa. (B) Size-exclusion chromatography analysis. The protein standards used are alcohol dehydrogenase (150 kDa), human serum albumin (66 kDa), and carbonic anhydrase (29 kDa). The *Zm*cbbF (red) was eluted just after the referenced human serum albumin (cyan) and far before carbonic anhydrase (blue). (For interpretation of the references to color in this figure legend, the reader is referred to the web version of this article.)

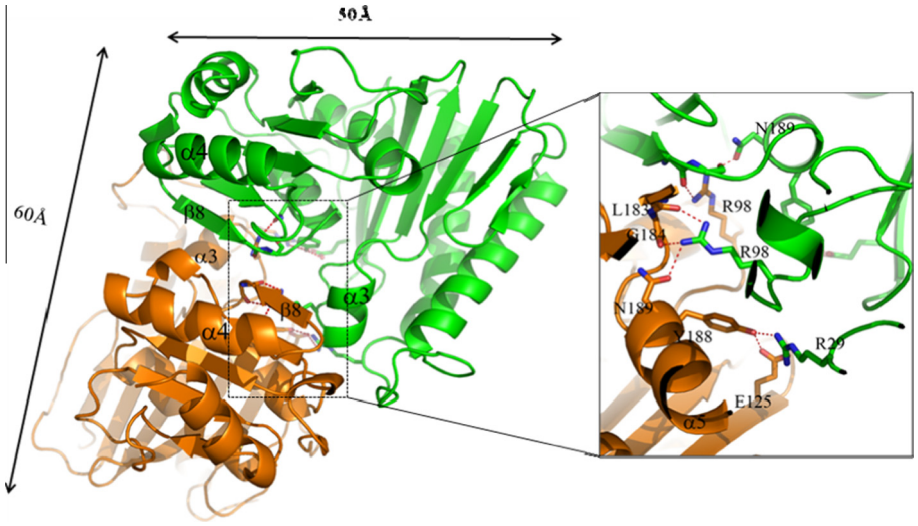

Fig. 4. The modeled dimeric structure. The dimeric *Zm*cbbF structure observed in the symmetry-related molecules was represented by ribbon diagram (left) and its dimeric interface was magnified (right). Each monomeric structure was differentiated by colors. Residues at the dimeric interface were displayed by stick models with hydrophilic interactions as red-dotted lines. The measured molecular size of the dimeric *Zm*cbbf structure along the longest and shortest axes was indicated. (For interpretation of the references to color in this figure legend, the reader is referred to the web version of this article.)

acid form two secondary elements of the α4-helix and the β8-strand in *Zm*cbbF (Fig. 2). Approximately thirty residues at the sequentially corresponding region of IMPases also form secondary structures of one α-helix and one β-strand [5,6]. In contrast, a simple loop is formed by less than fifteen residues in FBPases (Figs. 1A and 2), resulting in a large substrate-binding groove that is sufficient to accommodate a phosphate group at the C6-atom of an FBP substrate (PDB ID 4GBV) (Fig. 2B). On the other hand, the presence of α-helix (α4) and a β-strand (β8) in *Zm*cbbF and IMPases forms a relatively small groove at the structurally equivalent position (Fig. 2). Further, a hydrophobic Leu162 on the β7-α4 loop protrudes to this relatively small groove in *Zm*cbbF (Fig. 2B middle and C), indicating that a bulky charged group, for example, a phosphate at the C6-atom of FBP, is not favorable to bind to this small local hydrophobic pocket. Due to these discerned sequential and structural features, *Zm*cbbF is likely to belong to the IMPase protein family.

Second, the region covering Gly69-Asp78 in *Zm*cbbF (Fig. 1) forms secondary structures of β1 and β2 in other IMPases and FBPases (Fig. 2) and takes part in the catalysis directly through the Glu70 residue that interacts with the catalytic metal ion (Fig. 2). Unexpectedly, these residues were not traced in the current *Zm*cbbF structure that has no metal ion and a substrate (Fig. 1B). Similar disordered structures at the corresponding regions have also been reported in IMPase from *Aquifex aeolicus* VF5 (PDB ID 2PCR) and the dual specific IMPase/NADP(H) phosphatase from *Staphylococcous aureus* MSSA476 (PDB ID 3RYD) [21], indicating the presence of another highly flexible region in this family protein, in addition to the catalytic ML that has shown various spatial positions for either metal chelating or substrate binding [9]. The observed structural features suggest that the active site of this family protein would be re-arranged in a yet unreported way upon binding of a metal ion and a substrate or a product. Notably, the active site of the bi-functional FBPase from *Thermococcus neutrophilus* was re-organized upon binding of a substrate or a product with catalytic metal ions [22].

Accession codes

The coordinates for the structure have been deposited in the Protein Data Bank with an ID of 4n81.

Acknowledgments

This study was financially supported by Chonnam National University, 2011. We thank the staffs for the X-ray diffraction experiments at Beamline 5C SBII at the Pohang Accelerator in Korea.

References

[1] M.V. Bell, J.R. Dick, Molecular species composition of phosphatidylinositol from the brain, retina, liver and muscle of cod (*Gadus morhua*), Lipids 25 (1990) 691–694.
[2] F. Marcus, B. Gontero, P.B. Harrsch, J. Rittenhouse, Amino acid sequence homology among fructose-1,6-bisphosphatases, Biochem. Biophys. Res. Commun. 135 (1986) 374–381.
[3] M.J. Berridge, C.P. Downes, M.R. Hanley, Neural and developmental actions of lithium: a unifying hypothesis, Cell 59 (1989) 411–419.
[4] S.J. Pollack, J.R. Atack, M.R. Knowles, G. McAllister, C.I. Ragan, R. Baker, S.R. Fletcher, L.L. Iversen, H.B. Broughton, Mechanism of inositol monophosphatase, the putative target of lithium therapy, Proc. Natl. Acad. Sci. U.S.A. 91 (1994) 5766–5770.
[5] R. Bone, L. Frank, J.P. Springer, S.J. Pollack, S.A. Osborne, J.R. Atack, M.R. Knowles, G. McAllister, C.I. Ragan, H.B. Broughton, R. Baker, S.R. Fletcher, Structural analysis of inositol monophosphatase complexes with substrates, Biochemistry 33 (1994) 9460–9467.
[6] J.R. Atack, H.B. Broughton, S.J. Pollack, Structure and mechanism of inositol monophosphatase, FEBS Lett. 361 (1995) 1–7.
[7] B. Stec, H. Yang, K.A. Johnson, L. Chen, M.F. Roberts, MJ0109 is an enzyme that is both an inositol monophosphatase and the 'missing' archaeal fructose-1,6-bisphosphatase, Nat. Struct. Biol. 7 (2000) 1046–1050.
[8] K.A. Johnson, L. Chen, H. Yang, M.F. Roberts, B. Stec, Crystal structure and catalytic mechanism of the MJ0109 gene product: a bifunctional enzyme with inositol monophosphatase and fructose 1,6-bisphosphatase activities, Biochemistry 40 (2001) 618–630.
[9] K.A. Stieglitz, K.A. Johnson, H. Yang, M.F. Roberts, B.A. Seaton, J.F. Head, B. Stec, Crystal structure of a dual activity IMPase/FBPase (AF2372) from *Archaeoglobus fulgidus*. The story of a mobile loop, J. Biol. Chem. 277 (2002) 22863–22874.
[10] K.A. Stieglitz, M.F. Roberts, W. Li, B. Stec, Crystal structure of the tetrameric inositol 1-phosphate phosphatase (TM1415) from the hyperthermophile, *Thermotoga maritima*, FEBS J. 274 (2007) 2461–2469.
[11] Z. Li, K.A. Stieglitz, A.L. Shrout, Y. Wei, R.M. Weis, B. Stec, M.F. Roberts, Mobile loop mutations in an archaeal inositol monophosphatase: modulating three-metal ion assisted catalysis and lithium inhibition, Protein Sci. 19 (2010) 309–318.
[12] S. Lu, W. Huang, X. Li, Z. Huang, X. Liu, Y. Chen, T. Shi, J. Zhang, Insights into the role of magnesium triad in myo-inositol monophosphatase: metal mechanism, substrate binding, and lithium therapy, J. Chem. Inf. Model. 52 (2012) 2398–2409.
[13] J.S. Seo, H. Chong, H.S. Park, K.O. Yoon, C. Jung, J.J. Kim, J.H. Hong, H. Kim, J.H. Kim, J.I. Kil, C.J. Park, H.M. Oh, J.S. Lee, S.J. Jin, H.W. Um, H.J. Lee, S.J. Oh, J.Y. Kim, H.L. Kang, S.Y. Lee, K.J. Lee, H.S. Kang, The genome sequence of the ethanologenic bacterium *Zymomonas mobilis* ZM4, Nat. Biotechnol. 23 (1) (2005) 63–68.
[14] C. Aslanidis, P.J. de Jong, Ligation independent cloning of PCR products (LIC-PCR), Nucleic Acids Res. 20 (1990) 6069–6074.
[15] J. Jancarik, S.-H. Kim, Sparse matrix sampling: a screening method for crystallization of proteins, J. Appl. Crystallogr. 24 (1991) 409–411.
[16] Z. Otwinowski, W. Minor, Procession of X-ray diffraction data collected in oscillation mode, Methods Enzymol. 276 (1997) 307–326.
[17] P.D. Adams, P.V. Afonine, G. Bunkóczi, V.B. Chen, I.W. Davis, N. Echols, J.J. Headd, L.W. Hung, G.J. Kapral, R.W. Grosse-Kunstleve, A.J. McCoy, N.W. Moriarty, R. Oeffner, R.J. Read, D.C. Richardson, J.S. Richardson, T.C. Terwilliger, P.H. Zwart, PHENIX: a comprehensive Python-based system for macromolecular structure solution, Acta Crystallogr. D 66 (2010) 213–221.
[18] P. Emsley, K. Cowtan, Coot: model-building tools for molecular graphics, Acta Crystallogr. D 60 (2004) 2126–2132.
[19] I.W. Davis, L.W. Murray, J.S. Richardson, D.C. Richardson, MOLPROBITY: structure validation and all-atom contact analysis for nucleic acids and their complexes, Nucleic Acids Res. 32 (2004) W615–W619 (Web Server issue).
[20] S. Bhattacharyya, D. Dutta, B. Saha, A.K. Ghosh, A.K. Das, Crystal structure of Staphylococcal dual specific inositol monophosphatase/NADP(H) phosphatase (SAS2203) delineates the molecular basis of substrate specificity, Biochimie 94 (2012) 879–890.
[21] A.K. Brown, G. Meng, H. Ghadbane, D.J. Scott, L.G. Dover, J. Nigou, G.S. Besra, K. Fütterer, Dimerization of inositol monophosphatase *Mycobacterium tuberculosis* SuhB is not constitutive, but induced by binding of the activator Mg2+, BMC Struct. Biol. 7 (2007) 55–68.
[22] J. Du, R.F. Say, W. Lü, G. Fuchs, O. Einsle, Active site remodeling in the bifunctional fructose-6-bisphosphate aldolase/phosphatase, Nature 478 (2011) 534–537.